GaN-based p–i–n ultraviolet photodetectors with a thin p-type GaN layer on patterned sapphire substrates

Hongjuan Huang (黄红娟)[1], Dawei Yan (闫大为)[1*], Guosheng Wang (王国胜)[2], Feng Xie (谢 峰)[2], Guofeng Yang (杨国锋)[1], Shaoqing Xiao (肖少庆)[1], and Xiaofeng Gu (顾晓峰)[1]

[1]*Key Laboratory of Advanced Process Control for Light Industry (Ministry of Education), Department of Electronic Engineering, Jiangnan University, Wuxi 214122, Jiangsu, China*

[2]*The 38th Research Institute of China Electronics Technology Group Corporation, Hefei 230088, China*

[*]*Corresponding author: daweiyan@jiangnan.edu.cn*

Received April 18, 2014; accepted June 3, 2014; posted online August 11, 2014

We study the performance of GaN-based p–i–n ultraviolet (UV) photodetectors (PDs) with a 60 nm thin p-type contact layer grown on patterned sapphire substrate (PSS). The PDs on PSS exhibit a low dark current of ~2 pA under a bias of -5 V, a large UV/visible rejection ratio of ~7×10^3, and a high-quantum efficiency of ~40% at 365 nm under zero bias. The average quantum efficiency of the PDs still remains above 20% in the deep-UV region from 280 to 360 nm. In addition, the noise characteristics of the PDs are also discussed, and the corresponding specific detectivities limited by the thermal noise and the low-frequency $1/f$ noise are calculated.

OCIS codes: 230.0250, 230.5160, 230.5440.
doi: 10.3788/COL201412.092301.

Owning to the large light absorption coefficient of the direct bandgap, GaN-based semiconductors are ideal photodetector (PD) candidates, especially those operating in the ultraviolet (UV) region of the spectrum. The UV PDs have imperative applications in both the civilian and the military fields, such as missile-treating warning, biological agent detection, spatial optical communications, and UV imaging[1]. In the past decade, a variety of GaN-based PDs have been demonstrated[2–4]. The simplest one is of the photo-conductive type, whereas, the others require either a p–n junction or a Schottky barrier[5–7]. Among them, PDs based on the p–i–n structure have attracted intensive attention because they can offer high-quantum efficiency, high detectivity, and low dark current. However, for a conventional top-illuminated p–i–n structure, the performance of GaN-based PDs is usually limited by the following factors: 1) the strong absorption effect of the top p-type GaN contact layer, which can significantly reduce the possibility of the incident light penetrating into the absorption region, leading to a relatively low-quantum efficiency and 2) a high density of threading dislocations within the GaN films grown on frequently used sapphire substrates, which can provide additional paths for excess leakage current, resulting in severe reliability problems. Therefore, the performance of GaN-based p–i–n PDs can be further improved by thinning the p-type contact layer and improving the crystal quality of the GaN epi-layer. In this work, we fabricate the GaN p–i–n PDs on patterned sapphire substrate (PSS) through a lateral overgrowth-like process with only a 60 nm thin top p-type layer. The lateral epitaxial overgrowth (LEO) technology has been successfully used to produce low dislocation density areas on PSS[8–11]. It turns out that the PDs fabricated on PSS have a low dark current, a high-UV/visible rejection ratio, and a large quantum efficiency even in the photo-sensitive deep-UV range. We also discuss the noise characteristics of the PDs, and calculate the specific detectivities limited by the thermal and low-frequency noises, respectively.

Figure 1(a) shows the schematic cross section of the fabricated GaN p–i–n PDs prepared on PSS (Crystalwise Co). The epi-structure is grown by the metal-organic chemical vapor deposition method. To obtain crack-free films, a 2.25 μm undoped GaN buffer layer is grown on PSS. The p–i–n structure consists of a 1.75 μm n-type GaN layer (n~3×10^{18} cm^{-3}), a 400 nm undoped GaN photon absorption layer, and a 60 nm p-type GaN contact layer (p~7×10^{17} cm^{-3}). The full-width at half-maximum (FWHM) of the rocking curve of the (102) reflection is obviously narrower for the device structure grown on PSS (298 arcsec) than that grown on standard sapphire substrate (SSS) (396 arcsec), as shown in Fig. 2, indicating a decrease in the screw or edge-dislocation density in the films[12]. The standard photolithography and chlorine-based plasma dry etching processes are used to define and pattern the device mesa. The lift-off technique is employed to define the n-contact electrode region. A Ti/Al/Ni/Au (10/60/10/50 nm) metal stack

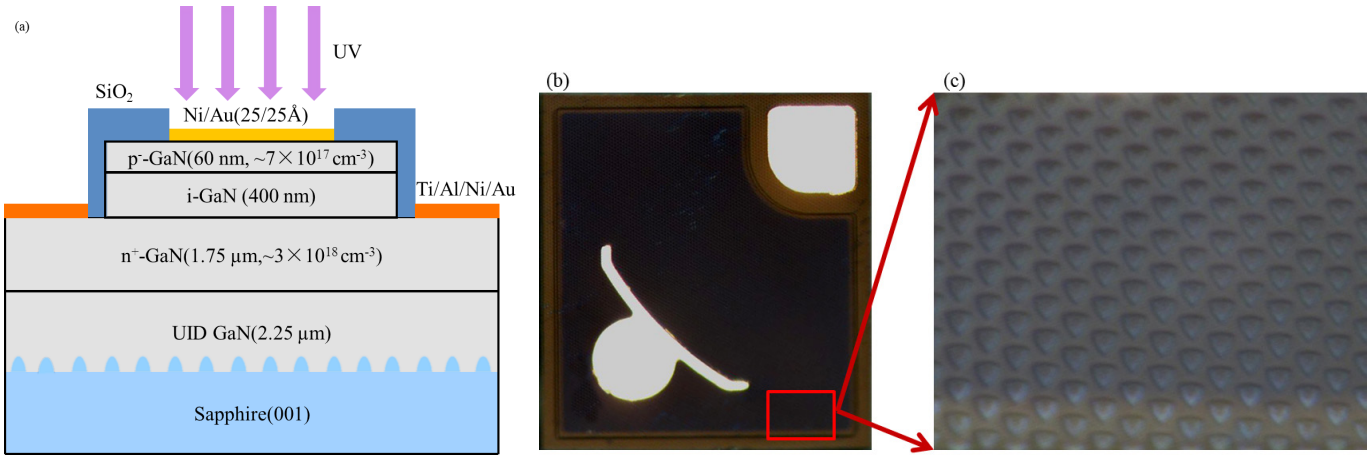

Fig. 1. (a) Schematic diagram of GaN-based p–i–n PD grown on PSS; (b) top view; (c) surface pattern optical images of the PSS.

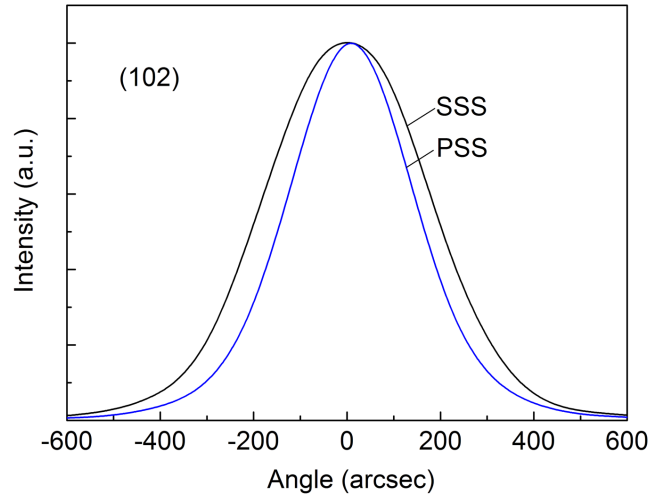

Fig. 2. XRD rocking curves of the (102) reflection for the device structures grown on PSS and SSS, respectively.

is deposited by e-beam evaporation, and immediately annealed using rapid thermal annealing in a N_2 environment at 750 °C for 1 min to form the ohmic contact. A thin Ni/Au (2/2 nm) layer is then evaporated on the mesa top to form the p-ohmic contact electrode after annealing at 500 °C for 300 s in air. Finally, the exposed semiconductor surface is covered by a SiO_2 dielectric layer, prepared by the plasma-enhanced chemical vapor deposition method. Figures 1(b) and (c) show the top view image and the micrograph of the GaN on PSS samples, respectively. The active area of the PDs is about 0.025 mm².

A Keithley 2636A sourcemeter is used to measure the current–voltage (I–V) characteristics of the PDs. A 500 W Xe lamp is used as the light source, and a monochromator is used for the single wavelength selection. An optical fiber is coupled onto the output port of the monochromator for the front-side illumination of the PDs, and an UV-enhanced Si photodiode (model S1226-5BQ) is used to calibrate the incident optical power.

Figure 3 shows the I–V curves of the GaN-based p–i–n PDs measured from 30 to 150 °C under the dark and illumination conditions, respectively. The dark curves feature typical rectifying behaviors of p–i–n junctions. At room temperature, the leakage current of the PDs is as low as ~2 pA at a reverse bias of 5 V, which is much smaller than that of conventional samples grown on SSS. This improvement can be attributed to the high crystal quality of the GaN epi-layers grown on PSS by LEO technology. The reverse dark current is obviously temperature dependent, and cannot be explained by the ideal p–n junction theory, and may be due to the thermal activation process of defect-related parasitic leakage current at high temperatures. The photocurrent, measured under the steady-state illumination with a monochromatic UV light of 365 nm and a power density of ~6.84 μW/mm², has only a slight increase in magnitude, which indicates that the thermally enhanced photo-carrier transport loss can be neglected in the PDs. In the forward bias direction, an exponential

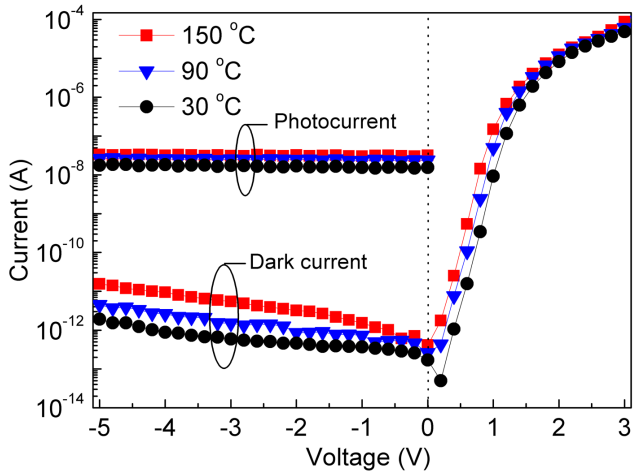

Fig. 3. Temperature-dependent I–V curves of GaN-based p–i–n PDs measured under dark and illumination conditions, respectively.

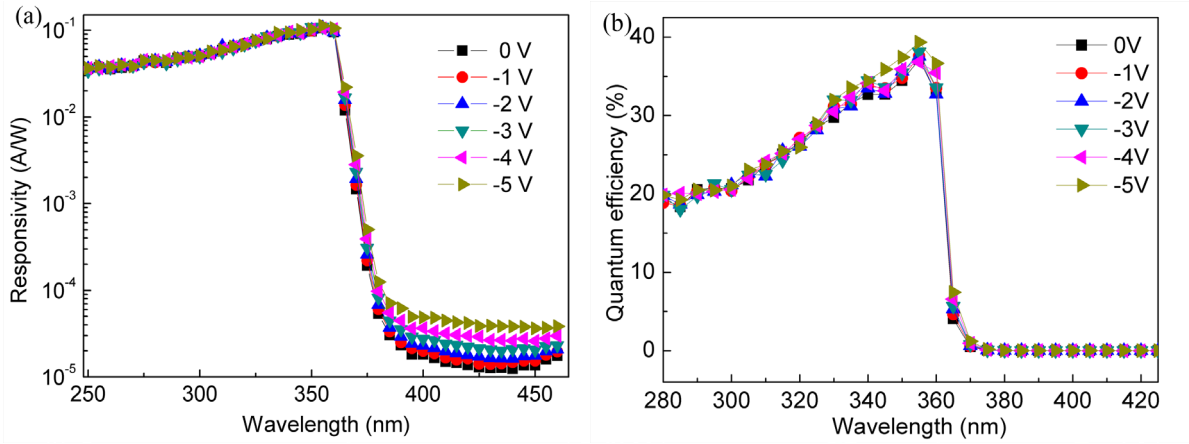

Fig. 4. (a) Spectral response characteristics of GaN-based p–i–n PDs measured under different reverse bias conditions at room temperature and (b) the derived quantum efficiency from 280 to 400 nm.

segment with an identical slope can be distinguished for each curve at low voltages, and the I–V relationship can be empirically represented by $I = I_o \exp(qV/nk_BT)$, where k_B is the Boltzmann constant, T is the absolute temperature, and n is the ideality factor determined from the current slopes. If n is between 1 and 2, the current flow is mainly the diffusion–recombination component. If n is larger than 2, the tunneling mechanism dominates the transport process. The value of n decreases from 3.2 to 1.9 when the temperature changes from 30 to 150 °C, suggesting that the carrier injection in the PDs is a combination of tunneling, diffusion, and recombination processes, and the contribution from diffusion to recombination component increases at elevated temperatures. We believe that the tunneling transport could be electrons tunnel from the n-type side of the junction to the p-type side via localized states within the bandgap of GaN, possibly following a staircase route similar to that in GaN-based LEDs[13].

Figure 4(a) shows the spectral response characteristics of the GaN-based p–i–n PDs as a function of the reverse bias with a bias step of -1 V, where the responsivity is obtained by the ratio of photocurrent I_p to the incident light power P_λ

$$R_\lambda = \frac{I_p}{P_\lambda} = \eta \frac{q\lambda}{hc}, \tag{1}$$

where η is the quantum efficiency, h is Plank's constant, c is the velocity of light, q is the electric charge, and λ is the wavelength of the incident light. As observed, the spectral curves gradually arise from 250 nm with a maximum value at ~360 nm, and then suffer from a rapid cut-off at ~365–380 nm (a result of the significant band-edge absorption of GaN). The PDs exhibit a larger UV/visible rejection ratio (defined as the responsivity at 360 nm divided by 450 nm) of ~7×10^3 at zero bias. Figure 4(b) shows the spectral quantum efficiencies of the PDs on PSS from 280 to 400 nm. The maximum quantum efficiency increases from 37% to 40% as the reverse bias increases from 0 to 5 V, which can be explained by the extension of the light absorption depletion region and the enhanced photocarrier collection efficiency under higher reverse biases. It is worth noting that the quantum efficiency of the PDs still remains above 20% in the deep-UV region from 280 to 360 nm in average, which is higher than the previously reported result of ~18%[14].

Next we will discuss the noise characteristics of the PDs on PSS, since the noise floor of the PDs limits the minimum detectable radiation power. For a PD operating at/near zero bias, the thermal noise usually dominates the dark current, which can be attributed to the random thermal motion of charged carriers, and can be expressed as

$$\left\langle I_n^2 \right\rangle = \frac{4k_BT}{R_0} B, \tag{2}$$

where $\langle I_n^2 \rangle$ is the total square noise current, R_0 is the differential resistance at zero bias, and B is the bandwidth of the PD filter. Then, the corresponding specific detectivity (D^*) limited by the thermal noise can be expressed as[15]

$$D^* = \frac{R_{\lambda 0}(A_0 B)^{1/2}}{\sqrt{\left\langle I_n^2 \right\rangle}} = R_{\lambda 0}\sqrt{\frac{R_0 A}{4k_BT}}, \tag{3}$$

where $R_{\lambda 0}$ is the zero-bias responsivity, and A is the active area of device. The R_0 value is determined as 4.5×10^{12} Ω from the dark I–V curve near zero bias, and the peak responsivity of R_λ is about 0.10622 A/W at zero bias from Fig. 4(a). Finally, substituting these values into Eq. (3), we can obtain D^*~2.76×10^{13} cm · Hz$^{1/2}$ · W^{-1}.

Another important noise component in the GaN-based p–i–n PDs is the $1/f$ noise, which usually dominates at low frequencies, and can be approximately described by[16]

$$S_n(f) = S_0 \frac{I_d^2}{f^\gamma}, \tag{4}$$

where $S_n(f)$ is the characteristic spectral density function, I_d is the dark current of the PDs, and S_0 and

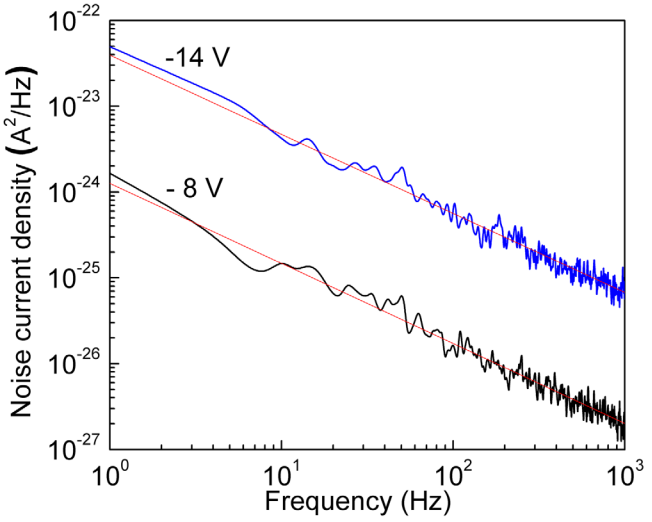

Fig. 5. Noise power spectra of GaN-based p–i–n PDs with an area of 1×1 (mm) measured from 1 to 1000 Hz at −8 and −14 V, respectively.

γ (typically close to unity) are the fitting parameters. Figure 5 shows the dark noise power spectra of the PDs with an area of 1×1 (mm) measured in a frequency range of 1–1000 Hz at −8 and −14 V, respectively. It turns out that the experimental data can be well fitted by Eq. (4), and the corresponding γ and S_0 values are derived to be around 0.93 and 1.5×10^{-2}, respectively. The $1/f$ noise could be closely related to the trap states in the wide bandgap GaN materials.

The noise equivalent power (NEP) describes the minimum detectable signal of PDs. It is defined as the incident optical power required to generate a photocurrent equal to the noise current at a given wavelength[17], and can be given by

$$\mathrm{NEP} = \frac{\sqrt{\langle i_n \rangle^2}}{R_\lambda}. \tag{5}$$

Here, the value of $<i_n>^2$ can be approximately determined by integrating the $S_n(f)$ function from 1 Hz to B[17]

$$\begin{aligned}\langle i_n \rangle^2 &= \int_0^B S_n(f)\mathrm{d}f \\ &= \int_0^1 S_n(f)\mathrm{d}f + \int_1^B S_n(f)\mathrm{d}f \\ &= S_0[\ln(B)+1],\end{aligned} \tag{6}$$

where it is assumed that $S_n(f) = S_0$, when $f < 1$ Hz. The corresponding specific detectivity D^* limited by the $1/f$ noise can be given by

$$D^* = \frac{\sqrt{A}\sqrt{B}}{\mathrm{NEP}}. \tag{7}$$

Thus, based on Figs. 4(a) and 5, the NEP and D^* are determined around 3.4×10^{-11} and 9.3×10^{10} cm · Hz$^{1/2}$ · W^{-1} at −8 V, respectively[15].

In conclusion, the performances of the GaN-based p–i–n PDs with a thin p-GaN layer grown on PSS are investigated. The PDs are demonstrated to possess a low dark current of ~2 pA at -5 V, a large UV/visible rejection ratio of $\sim7\times10^3$ at zero bias, and a high-quantum efficiency of ~40% at −5 V. Most importantly, the quantum efficiency of the PDs can still be higher than 20% even in the deep-UV region in average. The specific detectivities, limited by the thermal noise and the low-frequency $1/f$ noise, are determined to be $\sim2.76\times10^{13}$ cm·Hz$^{1/2}$·W^{-1} at 0 V and $\sim9.3\times10^{10}$ cm · Hz$^{1/2}$ · W^{-1} at −8 V, respectively.

This work was supported by the China Postdoctoral Science Foundation Funded Project (No. 2013M540437), the Natural Science Foundation of Jiangsu Province (No. BK2012110), the Joint Innovation Project of Jiangsu Province (No. BY2013015-19), and the Fundamental Research Funds for the Central Universities of China (Nos. JUSRP51323B and JUDCF13038).

References

1. M. Razeghi, Proc. IEEE **90,** 1006 (2002).
2. H. Jiang and T. Egawa, Appl. Phys. Lett. **90,** 121121 (2007).
3. J. Y. Duboz, N. Grandjean, F. Omnes, M. Mosca, and J. L. Reverchon, Appl. Phys. Lett. **86,** 063511 (2005).
4. Y. Zhang, S. C. Shen, H. J. Kim, S. Choi, J. H. Ryou, R. D. Dupuis, and B. Narayan, Appl. Phys. Lett. **94,** 221109 (2009).
5. F. Xie, H. Lu, D. J. Chen, X. Q. Xiu, H. Zhao, R. Zhang, and Y. D. Zheng, IEEE Electron. Device Lett. 32, 1260 (2011).
6. T. Tut, T. Yelboga, E. Ulker, and E. Ozbay, Appl. Phys. Lett. **92,** 103502 (2008).
7. J. K. Sheu, M. L. Lee, C. J. Tun, and S. W. Lin, Appl. Phys. Lett. **88,** 043506 (2006).
8. Y. Z. Chiou, Y. G. Lin, and T. K. Ko, Semicond. Sci. Technol. **24,** 055004 (2009).
9. D. S. Wuu, W. K. Wang, W. C. Shih, R. H. Horng, C. E. Lee, W. Y. Lin, and J. S. Fang, IEEE Photon. Technol. Lett. **17,** 288 (2005).
10. S. J. Chang, Y. D. Jhou, Y. C. Lin, S. L. Wu, C. H. Chen, T. C. Wen, and L. W. Wu, IEEE Photon. Technol. Lett. **20,** 1866 (2008).
11. G. S. Wang, H. Lu, D. J Chen, F. F. Ren, R. Zhang, and Y. D. Zheng, IEEE Photon. Technol. Lett. 25, 652 (2013).
12. B. Heying, X. H. Wu, S. Keller, Y. Li, D. Kapolnek, B. P. Keller, S. P. DenBaar, and J. S. Speck, Appl. Phys. Lett. **68,** 643 (1996).
13. D. W. Yan, H. Lu, D. J. Chen, R. Zhang, and Y. D. Zheng, Appl. Phys. Lett. **96,** 083504 (2010).
14. J. C. Lin, Y. K. Su, S. J. Chang, W. H. Lan, W. R. Chen, K. C. Huang, Y. C. Cheng, and W. J. Lin, IEEE Photon. Technol. Lett. **20,** 1255 (2008).
15. T. Li, D. J. H. Lambert, M. M. Wong, C. J. Collins, B. Yang, A. L. Beck, U. Chowdhury, R. D. Durpuis, and J. C. Campbell, Opt. Quant. Electron. **37,** 538 (2001).
16. D. V. Kuksenkov, H. Temkin, A. Osinsky, R. Gaska and M. A. Khan, J. Appl. Phys. **83,** 2142 (1998).
17. J. L. Hou, S. J. Chang, M. C. Chen, C. H. Liu, T. J. Hsueh, J. K. Sheu, and S. G. Li, IEEE Trans. Electron. Devices **60,** 1178 (2013).